International Journal of Pharmaceutics 682 (2025) 125930

Contents lists available at ScienceDirect

International Journal of Pharmaceutics

journal homepage: www.elsevier.com/locate/ijpharm

Silk fibroin microparticles as a candidate for wound healing applications: evaluating the role of adenosine

Beatriz G. Bernardes [a,b], Rossella Laurano [c], Clara López-Iglesias [b], Rui Magalhães [a], Raquel Costa [a], Carlos A. García-González [b], Ana Leite Oliveira [a,*]

[a] Universidade Católica Portuguesa, CBQF – Centro de Biotecnologia e Química Fina – Laboratório Associado, Escola Superior de Biotecnologia, Porto, Portugal
[b] AerogelsLab, Department of Pharmacology, Pharmacy and Pharmaceutical Technology, I+D Farma group (GI-1645), iMATUS and Health Research Institute of Santiago de Compostela (IDIS), Universidade de Santiago de Compostela E-15782 Santiago de Compostela, Spain
[c] Department of Mechanical and Aerospace Engineering, Politecnico di Torino, Corso Duca degli Abruzzi 24, 10129 Torino, Italy

ARTICLE INFO

Keywords:
Bioaerogels
Silk fibroin
Tissue regeneration
Adenosine

ABSTRACT

In this study, silk fibroin (SF) aerogel microparticles were developed as a delivery system for adenosine (ADO) to exploit its anti-inflammatory and regenerative properties for wound healing. Supercritical CO_2 drying was used to prepare ADO-loaded SF aerogel microparticles with different SF concentrations (3 %, 5 %, 7 % w/v) and SF:ADO ratios (10:1, 5:1, 2:1). Characterization revealed high porosity (91–94 %), interconnected pores, high skeletal density (1.22–1.32 g/cm^3) and significant surface area (191–306 m^2/g). Notably, the 5 % SF with a 5:1 SF:ADO ratio emerged as the most promising formulation, exhibiting excellent morphological and biological properties (91 % porosity, 1.31 g/cm^3 skeletal density, and 191 m^2/g surface area). *In vitro* studies on human dermal fibroblasts (HDF), keratinocytes (HaCaT), and human dermal microvascular endothelial cells (HDMEC) demonstrated enhanced viability and proliferation in HDF and HaCaT cells. Specifically, the 5 % SF 5:1 and 5 % SF 2:1 formulations significantly boosted proliferation (over 100 % compared to control) for up to 7 days, highlighting their potential. While HDMECs showed sensitivity to higher ADO concentrations (observed with the 5 % SF 2:1 formulation), the 5 % SF 5:1 formulation achieved the most balanced cellular response across all cell types, underscoring the importance of precise dosage. These findings support the potential of ADO-loaded SF aerogel microparticles in tissue regeneration applications. Further *in vivo* studies are needed to validate therapeutic efficacy and benchmark against existing wound healing treatments.

1. Introduction

The wound healing process is a complex, sequential cascade encompassing haemostasis, inflammation, proliferation, and remodelling/maturation. When this natural progression is disrupted, a wound can become chronic, leading to a continuous inflammatory process and consequently to impaired healing (Bernardes et al., 2021). While exudate is critical for healing, as it delivers essential nutrients and leukocytes, chronic wound exudates contain elevated levels of proteases and enzymes that hinder cell proliferation, degrade growth factors, and damage the extracellular matrix, leading to tissue degradation and prolonged inflammation (Bernardes et al., 2021).

In recent years, bio-based aerogels derived from natural polymers have gained attention in wound healing applications due to their high porosity, extensive surface area and excellent biocompatibility, enabling advanced performance in fluid transfer and bioactive compound delivery (López-Iglesias et al., 2019; Soorbaghi et al., 2019). Among the proposed biopolymers, silk fibroin (SF), a protein that can be industrially obtained from *Bombyx mori* silk, stands out for its biocompatibility, biodegradability, and ability to stabilize and preserve bioactive compounds (Bernardes et al., 2024; Li et al., 2015). Additionally, SF has shown potential to support cell proliferation and promote tissue regeneration, making it an ideal material for wound healing applications (Bernardes et al., 2024; Li et al., 2015; Sultan et al., 2018:; Yousaf et al., 2020). SF aerogels offer a promising platform for wound healing and tissue regeneration due to their antioxidant properties, sustained degradation, high porosity, specific surface area, and ability to incorporate therapeutic agents (Bernardes et al., 2024; Marin et al., 2014; Mallepally et al., 2015; Bernardes et al., 2023; Mallepally et al., 2014).

Adenosine, a nucleoside composed of adenine linked to ribose (ADO,

* Corresponding author.
E-mail addresses: carlos.garcia@usc.es (C.A. García-González), aloliveira@ucp.pt (A.L. Oliveira).

https://doi.org/10.1016/j.ijpharm.2025.125930
Received 30 April 2025; Received in revised form 20 June 2025; Accepted 2 July 2025
Available online 3 July 2025
0378-5173/© 2025 The Authors. Published by Elsevier B.V. This is an open access article under the CC BY license (http://creativecommons.org/licenses/by/4.0/).

$C_{10}H_{13}N_5O_4$), plays an essential role in various physiological processes, including ATP synthesis and cellular energy transfer. In the context of wound healing, ADO has been shown to be highly effective in reducing inflammation and promoting tissue repair (Haskó and Cronstein, 2013). Four ADO receptor subtypes (A_1, A_{2A}, A_{2B}, A_3) regulate a diversity of cellular responses, with A_{2A} playing a central role in mediating anti-inflammatory, angiogenic, and collagen production (Wilson et al., 2009; Perez-Aso et al., 2014). ADO activation of A_{2A} receptors enhances extracellular matrix synthesis and promotes dermal regeneration by stimulating collagen production, angiogenesis, and interleukin (IL)-13 production (Montesinos et al., 2002; Montesinos et al., 2015; Cronstein, 2004; Squadrito et al., 2017; Chen et al., 2024). A_{2B} receptor activation reduces endothelial inflammation and promotes angiogenesis by stimulating endothelial proliferation and the release of VEGF and basic fibroblast growth factor (bFGF), aiding tissue repair and wound healing (Haskó et al., 2009). By binding to A_2 receptors, ADO stimulates endothelial cell migration, proliferation, and secretion of vascular endothelial growth factor (VEGF) *in vitro* (Montesinos et al., 2002; Borges et al., 2021). Recent studies demonstrate the effectiveness of topical ADO A_{2A} receptor agonists in accelerating wound closure and healing in both normal and diabetic animal models, underscoring ADO's therapeutic potential (Montesinos et al., 2002; Montesinos et al., 2015; Montesinos et al., 1997). The multifaceted properties of ADO make it a valuable molecule for therapeutic interventions, aimed at promoting wound healing and repair.

The primary challenge with ADO in *in vivo* applications is its short half-life (less than 10 s), which leads to rapid clearance from circulation, mainly due to cellular uptake by erythrocytes and vascular endothelial cells (Kazemzadeh-Narbat et al., 2015). Therefore, it is important to develop drug carriers that can effectively function as protective barriers. ADO carrier strategies for skin delivery include alginate beads containing monoolein polar lipid (Ng et al., 2017), chitosan nanoparticles (Kazemzadeh-Narbat et al., 2015), novel nanostructured lipid carrier (Gomes Daré et al., 2024) and SF particles (Pritchard et al., 2010). In the case of the lipid carrier, it was used to co-encapsulate simvastatin and ADO for topical delivery to address the healing of chronic and hard-to-heal wounds. The resulting system had superior stability, enhanced cellular biocompatibility, improved skin drug retention, as well as effective promotion of cell proliferation and migration in the presence of ADO (Gomes Daré et al., 2024). Monoolein-alginate beads offer a promising approach for wound care by improving exudate absorption and enabling localized ADO delivery for enhanced healing (Ng et al., 2017). Some authors have developed silk-based polymers as drug-release carriers of ADO (Pritchard et al., 2010; Szybala et al., 2009; Wilz et al., 2008). In one example, solid ADO powder reservoirs layered with eight coats of 8 % SF (w/v) demonstrated a consistent linear release profile, maintaining ADO release over 14 days (Pritchard et al., 2010). This study proposes to develop SF aerogel particles as an controlled release system for ADO through aerogel technology. These microparticles are expected to provide a combined two-step (prompt plus sustained) ADO release profile at the wound site, promoting angiogenesis and accelerating wound healing by targeting ADO receptors and leveraging the unique properties of SF aerogels. Supercritical fluid technology, is a promising and sustainable tool for the production of innovative bioaerogels, allowing precise control over the structure, properties and composition of the material, guaranteeing optimised and personalised results for various biomedical applications (Bernardes et al., 2021). In this study, SF aqueous solutions with varying concentrations (3, 5 and 7 % SF (w/v)) and SF:ADO weight ratios (10:1, 5:1 and 2:1), were processed into alcogel particles and then dried using supercritical CO_2 under optimized time (3.5 h), temperature (40 °C), and pressure conditions (120 bar). The obtained aerogel particles were characterized regarding their physicochemical properties and drug release kinetics. The *in vitro* biological interaction between ADO-loaded SF aerogel particles and key cell types involved in wound healing and regeneration processes where studied, namely: primary human dermal fibroblasts (HDF), human keratinocytes (HaCaT), and human dermal microvascular endothelial cells (HDMEC). This study compares the ADO's effects on these three cell types which play crucial role during the wound healing process and tissue regeneration, when administered as a therapeutic agent, rather than solely considering its natural role in cellular pathways.

2. Experimental

2.1. Materials and Reagents

SF was extracted from *B. mori* cocoons provided by the Portuguese Association of Parents and Friends of Mentally Disabled Citizens (APPACDM, Porto, Portugal). Sodium carbonate anhydrous (Na_2CO_3) (≥99.8 %), lithium bromide (LiBr) (≥99 %) and absolute ethanol (≥99.8 %) were obtained from Honeywell (Wabash, IN, USA). Span® 80 (428.62 g/mol) and ADO (≥99 %; CAS: 68–51-7) were purchased from Sigma Aldrich (St. Louis, MO, USA). Flash Phalloidin Green 488 and DAPI was purchased from Biolegend (San Diego, CA, USA). The CO_2 (99.995 % purity) was provided by GASIN (Leça da Palmeira, Portugal).

2.2. Preparation of silk fibroin aerogel particles

SF was extracted from *B. mori* silkworm cocoons following the previous reported methodology (Bernardes et al., 2023). To prepare ADO-loaded SF aerogel microparticles (ADO-SF), SF solutions of different concentrations (3 %, 5 %, and 7 % w/V) were mixed with ADO at different weight ratios (10:1, 5:1 and 2:1). ADO was incorporated into the SF solution at 50 °C gently stirring for 5 min to achieve ADO dissolution and a uniform dispersion. Then, alcogel particles were prepared at the different concentrations and SF:ADO ratios, according to a modified method previously developed (Bernardes et al., 2023). Briefly, SF gel particles were centrifuged at 5000 rpm for 15 min to remove water, then transferred to 40 mL of absolute ethanol. After 3 h, a second ethanol exchange ensured the water removal, yielding alcogel particles. To produce aerogels, alcogel particles were subjected to supercritical CO_2 drying using an equipment from Parr Instrument Company (Moline, Illinois, USA). The process was conducted at 40 °C with a continuous CO_2 flow of 15 mL/min. Initially, the system was maintained at 120 bar for 2.5 h, followed by a 1.5 h batch phase at 130 bar. Drying was completed with a final continuous phase of 1 h at 125 bar and 10 mL/min. This procedure effectively removed ethanol, yielding stable ADO-SF microparticles (Bernardes et al., 2023). The obtained particles were denoted as X%SF Y:1 (SF:ADO), where X%SF represents the SF concentration (3, 5, or 7 % w/v), and Y:1 indicates the SF-to-ADO weight ratio (10:1, 5:1, or 2:1). SF aerogel without ADO were labelled solely by their SF concentration (e.g., 3 %SF, 5 %SF, 7 %SF). A schematic illustration of the methodology is presented in Fig. 1.

2.3. Physicochemical properties

The morphology of the ADO-SF aerogel microparticles was analysed by Scanning Electron Microscopy (SEM) analysis. ADO-SF aerogel microparticles were dispersed and fixed on sample holders with double-sided adhesive carbon tape (NEM tape; Nisshin, Japan), followed by sputter-coating with a 9–12 nm layer of gold/palladium (Polaron, Bad Schwalbach, Germany). Finally, the samples were examined using a Phenom Pro G6 SEM (Thermo Fisher Scientific, Eindhoven, The Netherlands) at 10 kV with the backscattered electron detector (BSD).

The particle sizes of ADO-SF microparticles were measured using a particle size analyzer Mastersizer 3000E (Malvern Panalytical, Malvern, UK) with the obtained data processed following the Mie Theory (Bernardes et al., 2023). The skeletal density (ρ_{skel}) of ADO-SF microparticles was determined using helium pycnometry (MPY-2, Quantachrome, Delray Beach, FL, USA) at 25 °C and 1.03 bar, with each measurement conducted in triplicate. Particle size distributions were

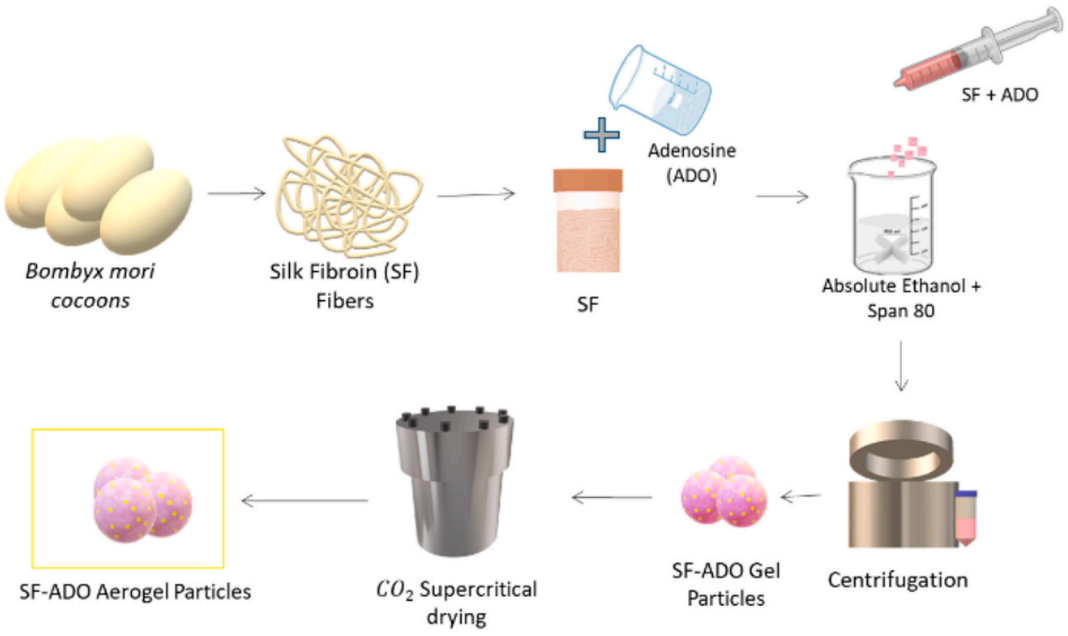

Fig. 1. Schematic illustration of the procedure for preparing the ADO-SF microparticles.

reported by parameters based on the maximum particle size for a given percentile of the sample volume (Dv10, Dv50, and Dv90).

The tapped density (ρ_{tapped}) of ADO-SF microparticles was calculated as the weight-to-volume ratio after tapping at 22–23 S per minute. Considering the 74 % packing efficiency of aerogel particles, the envelope density (ρ_{env}) was determined by adjusting for the 26 % void space. These measurements followed a method adapted from our previous research (Bernardes et al., 2023). In this approach, 26 % of the total particle bed volume was considered as vacant space. This vacant volume was subtracted from the total tapped volume to calculate ρ_{env}. The porosity (ε) of the aerogels was calculated as a percentage from the ρ_{skel} and ρ_{env} (Bernardes et al., 2023). The textural and morphological characteristics of the ADO-SF microparticles were analysed via nitrogen adsorption–desorption using an ASAP 2000 instrument (Micromeritics, Norcross, GA, USA). The specific surface area (a_{BET}) was calculated using the Brunauer-Emmet-Teller (BET) method. The Barrett-Joyner-Halenda (BJH) method was employed to analyze pore size distribution, as well as to determine the total specific pore volume (Vp,BJH) and average pore diameter (Dp,BJH) from the desorption branch of the N_2 isotherm. In the mesopore range (2–50 nm), mesopore volume (V_{mes}) was extracted from cumulative BJH pore volume profiles. The macropore volume (V_{mac}) was calculated by subtracting the V_{mes} from the total specific pore volume (i.e. the reciprocal of the ρ_{env}) (López-Iglesias et al., 2019).

Fourier Transform Infrared with Attenuated Total Reflectance (FTIR-ATR) spectroscopy was used to assess the secondary structure formation, conformational changes and chemical structure of ADO-SF microparticles. The FTIR-ATR analysis was performed on a Perkin Elmer spectrometer, Spectrum 100 (Waltham, MA, USA), equipped with an ATR sampling accessory (PIKE Technologies, Beaconsfield, UK) and a diamond/ZnSe crystal. For each sample, 32 scans were collected at a resolution of 4 cm^{-1} across the 1200–2000 cm^{-1} wavenumber range. Baseline adjustment and spectra normalization were performed to ensure accuracy.

Differential scanning calorimetry (DSC) was used to examine the thermal properties of ADO-SF microparticles. The analysis was conducted using a Netzsch DSC 204 F1 Phoenix equipment (NETZSCH, Selb, Germany). Approximately 2.0 mg of the aerogel samples were weighed on an aluminium pan and stabilized overnight at 40 °C before analysis. The sample was then heated from 30 °C to 350 °C at a rate of 10 °C/min under a nitrogen flow rate of 20 mL/min. Each measurement was performed in triplicate, with the results representing the average of the three analyses.

2.3.1. Adenosine release and loading capacity evaluation

To determine the ADO release profile and loading capacity, 20 mg of ADO-SF microparticles were suspended in phosphate-buffered saline (PBS, pH 7.4) at a concentration of 0.7 mg/mL and incubated at 37 °C with agitation at 100 rpm. Aliquots of 1 mL were collected at predetermined intervals (5, 30 min, 1, 2, 4, and 6 h), and replaced each time with an equal volume of fresh PBS to maintain a constant volume in the release medium.

To quantify the total ADO content in the ADO-SF microparticles, 20 mg of particles were accurately weighed and incubated in PBS (pH 7.4) medium at 37 °C with continuous agitation, at 100 rpm for 2 h, to facilitate complete ADO release. After incubation, the samples were centrifuged at 11,000 rpm for 20 min at 4 °C to ensure the release of free ADO from the particles. Then, the ADO loading and the entrapment yield were calculated using Eqs. (1) and (2) (López-Iglesias et al., 2019), respectively:

$$Loading(\%) = \frac{w_P}{w_{aer}} \times 100 \quad (1)$$

$$Entrapmentyield(\%) = \frac{w_P}{w_i} \times 100 \quad (2)$$

Where w_P is the final amount (in mg) of ADO obtained by HPLC measurements, w_{aer} is the total weight of the aerogel particles (mg), and w_i is the initial amount (mg) of ADO added for the particles' preparation.

ADO concentrations were analysed using High-Performance Liquid Chromatography (HPLC)-DAD (Agilent 1260 Infinity II, Agilent, Santa Clara, CA, USA) adapted from a previously established procedure (Marin et al., 2007). Chromatographic separation was achieved on a ZORBAX Eclipse XBD-C18 column (4.6 × 250 mm, 5 μm, Agilent, Santa Clara, CA, USA) with a mobile phase of 10 % (v/v) acetonitrile in water, at a flow rate of 0.8 mL/min, and detection at 260 nm. Calibration was based on ADO standards ranging from 0.5–100 μg/mL ($R^2 = 0.999$).

2.3.1.1. Adenosine loss quantification during centrifugation process. The ADO-SF microparticles were produced using a two-step centrifugation process followed by supercritical CO_2 drying. To evaluate potential ADO

loss during solvent exchange process, additional quantifications were performed to evaluate the ADO mass balance in the process. Although ADO is generally insoluble in ethanol, losses may still occur during the water-to-ethanol exchange within the particles. After each centrifugation step, a 2-mL aliquot of the supernatant was collected and dried in an Eppendorf tube at 50 °C for two days. The amount of ADO was determined by measuring the resulting dry weight. The dry weight of the particles without ADO was used as a blank. The total ADO loss was calculated by measuring the ethanol volume remaining after centrifugation (excluding the particle volume).

2.4. In vitro cell viability and cell behavior

2.4.1. Cell seeding

To assess cell viability and proliferation, Human keratinocyte cell line (HaCat), Human Dermal Fibroblasts (HDF) and Human Dermal Microvascular Endothelial Cells (HDMEC) were used to evaluate the effects of ADO-SF microparticles on different skin cell types, considering their roles in wound healing, vascular stability, and epidermal barrier maintenance. HaCat cells was obtained from Cell Line Services (Oppenheim, Denmark). HDF (P10858) and HDMEC (P10861) cells were obtained from Innoprot (Bizkaia, Spain). HDF, HaCaT, and HDMEC were seeded in 96-well plates at respective densities of 1.0×10^5, 5.0×10^4, and 2.0×10^4 cells/mL. For SEM analysis, HaCaT cells were seeded at 2.5×10^4 cells/mL, while for fluorescence microscopy, densities of 5.0×10^4 cells/mL for HDF, 2.5×10^4 cells/mL for HaCaT, and 2.0×10^4 cells/mL for HDMEC were used. Cell density was adjusted according to the proliferation rates of each cell type, with higher seeding for faster-growing HaCaT cells and lower density for HDMECs to avoid contact inhibition (Marks et al., 1985). The culture medium for HDF and HaCaT cells was Dulbecco's Modified Eagle's Medium (DMEM; Gibco™ DMEM, high glucose) supplemented with 10 % fetal bovine serum (FBS; Bio-West) and 1 % penicillin–streptomycin (Lonza, Basel, Switzerland). HDMECs were cultured in Endothelial Cell Medium Kit (Innoprot, Derio, Spain). The plates were incubated at 37 °C in a humidified atmosphere with 5 % CO_2 for 24 h.

2.4.2. Adenosine conditioned media

The MTT (methyl thiazolyl tetrazolium) assay was employed to assess cell viability when cells were exposed to ADO solutions at varying concentrations (Bernardes et al., 2023). Cells were exposed to ADO solutions at varying concentrations (0.1 to 2 mg/mL), and samples were collected at 1, 2, and 3 days for MTT analysis. The experimental setup included negative and positive controls, as well as medium blanks.

2.4.3. Resazurin and BrdU incorporation assays

To assess cell metabolic activity and proliferation in the presence of ADO-SF microparticles, after 24 h, 72 h and 7 days, the particles were sterilized by UV radiation for 20 min, suspended in complete culture medium (5 mg/mL), and added to each well in triplicate. Cell viability was quantified using the resazurin assay by adding 200 μL of resazurin solution (0.1 mg/mL) to each well and incubating for 2 h, followed by fluorescence measurement (excitation 530 nm, emission 590 nm) with a microplate reader (Synergy Mx, Biotek, Santa Clara, CA, USA). Cell proliferation was evaluated using a BrdU (bromodeoxyuridine) incorporation assay (Cell Proliferation ELISA BrdU (colorimetric), Roche Diagnostics, Mannheim, Germany), following the prior methodology (Bernardes et al., 2023).

2.4.4. Cell morphology

For SEM analysis, cells cultured on tissue culture plates (TCPs) with ADO-SF microparticles were washed with PBS and fixed for 30 min with 2.5 % glutaraldehyde in PBS (pH 7.4). The sample drying method followed the previous described procedure (Bernardes et al., 2023). The samples were then fixed on sample holders with double-sided adhesive carbon tape (NEM tape; Nisshin, Japan), followed by sputter-coating with a 9–12 nm layer of gold/palladium (Polaron, Bad Schwalbach, Germany). Finally, the samples were examined using a Phenom Pro G6 SEM (Thermo Fisher Scientific, Eindhoven, Netherlands) at 5 kV with the secondary electron detector (SED).

To evaluate cell morphology, samples were subjected to staining for filamentous actin (F-actin) and nuclei (DAPI). After fixation with 4 % vol. formaldehyde and permeabilization with 0.5 % Triton X-100, samples were blocked with 5 % vol. FBS to prevent non-specific binding. The stained samples were then observed using an inverted microscope Axio Vert A1 FL (ZEISS, Oberkochen, Germany), equipped with an LED light source and the X-Cite Xylis (D) illumination system. Images were captured using a ZEISS Axiocam 305 color digital camera and processed with ZEN Microscopy Software (ZEISS, Oberkochen, Germany).

2.5. Statistical analysis

Quantitative data were subjected to an analysis of variance (one-way ANOVA) followed by a post hoc Tukey's test, using a level of significance (α) of 0.05. For non-normally distributed data, the Kruskal-Wallis non-parametric test was used, with a significance level (α) of 0.05. Statistical analyses were performed using GraphPad Prism v. 9.3.1 (GraphPad Software, La Jolla, CA, USA).

3. Results

3.1. Morphological, textural and chemical characterization of ADO-SF microparticles

Fig. 2 is a representative image of the developed ADO-SF aerogel microparticles, which have a rough and textured surface and exhibit different shapes, from spherical to more irregular. The particle size distribution of the ADO-SF microparticles is shown in Table 1.

Dv50 represents the median particle size, indicating that 50 % of the particles are smaller than this value. For 3 % and 7 % ADO-SF microparticles, a decrease in ADO concentration corresponds to a reduction in particle size, suggesting that higher ADO content may promote aggregation or structural changes, as shown on Fig. 2. However, 5 % SF particles deviate from this trend, showing an increase in diameter as ADO concentration decreases. Span values offer insights into particle size distribution, where a span value around 1 indicates a narrow, uniform distribution, while higher values suggest broader variability. Most ADO-SF microparticles formulations exhibit span values close to 1, suggesting consistent particle sizes. However, the 7 % SF formulations with ADO display broader size distributions, as evidenced by span values of approximately 2. This suggests that the balance between SF concentration and ADO affects particle uniformity, with higher SF and moderate ADO levels resulting in less consistent sizes. Variability in particle size could impact ADO release, as uniform particles may offer a more predictable release profile.

Data on ρ_{skel}, ρ_{env} and ε of ADO-SF microparticles in Table 2 provide insights into their physical characteristics across various formulations. ρ_{skel} and ρ_{env} values are relatively consistent, with a range of 1.22 to 1.32 g/cm^3 and 0.07 to 0.11 g/cm^3, respectively. It is noteworthy that in the 3 % SF and 7 % SF formulations, the highest ρ_{skel} is observed in samples without ADO. For 3 % SF, the pure SF formulation (1.32 g/cm^3) had the highest skeletal density, while ADO incorporation lowered ρ_{skel} to 1.22–1.26 g/cm^3. For 5 % SF, density ranged from 1.22 to 1.31 g/cm^3, with the 5:1 formulation (1.31 g/cm^3) being significantly higher. In 7 % SF, most formulations were statistically similar, except 10:1 (1.22 g/cm^3), which was significantly lower. The 10:1 formulations across all SF concentrations had a consistent density (1.22 g/cm^3), while 5 % SF 5:1 showed a significantly higher value than 3 % SF 5:1. No significant differences were observed for 2:1 formulations. ρ_{env} remained stable (0.07–0.11 g/cm^3) across all formulations, showing no significant differences. This indicates that ADO incorporation does not impact the external density of the microparticles. Similarly, ε remained consistent

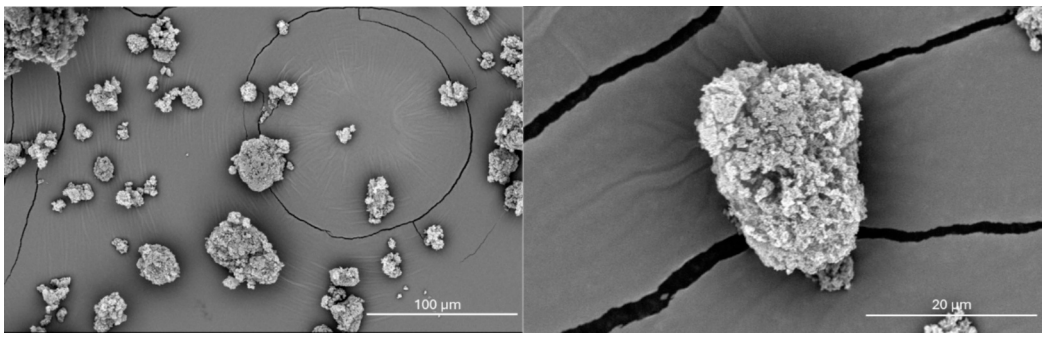

Fig. 2. Representative SEM images of SF aerogel microparticles at 1500x and 5000x magnification, respectively.

Table 1
Particle size distribution parameters, namely Dv10, Dv50, Dv90, and Span, assessed for aerogel ADO-SF microparticles.

	ADO-SF microparticles			
	Dv10 (µm)	Dv50 (µm)	Dv90 (µm)	Span
3 %SF	8.8 ± 0.01	19.4 ± 0.03	37.8 ± 0.26	1.5
3 %SF 10:1	6.9 ± 0.02	15.1 ± 0.08	30.6 ± 0.63	1.6
3 %SF 5:1	7.6 ± 0.01	16.2 ± 0.04	31.4 ± 0.28	1.5
3 %SF 2:1	10.2 ± 0.11	23.5 ± 0.53	48.1 ± 4.92	1.6
5 %SF	9.3 ± 0.08	22.4 ± 0.06	46.1 ± 1.21	1.6
5 %SF 10:1	8.6 ± 0.01	17.8 ± 0.04	33.5 ± 0.23	1.4
5 %SF 5:1	7.7 ± 0.00	17.2 ± 0.02	34.1 ± 0.13	1.5
5 %SF 2:1	5.9 ± 0.03	12.1 ± 0.04	24.8 ± 0.39	1.6
7 %SF	7.7 ± 0.01	17.4 ± 0.04	35.9 ± 0.35	1.6
7 %SF 10:1	9.3 ± 0.05	22.4 ± 0.26	55.6 ± 2.78	2.1
7 %SF 5:1	7.2 ± 0.01	17.2 ± 0.08	42.8 ± 1.02	2.1
7 %SF 2:1	6.7 ± 0.01	14.2 ± 0.05	33.6 ± 0.69	1.9

Table 2
Characterization of ADO-SF microparticles. Notation: Results were statistically compared. Identical letters (a, b) indicate statistically homogeneous groups for SF concentration without ADO. Identical symbols (*, #) indicate homogeneity among different SF concentrations with the same ADO:SF ratio. ρ_{skel} - (ANOVA $\alpha < 0.05$); ρ_{env} (Kruskall-wallis $\alpha < 0.05$).

Particles	ρ_{skel} (g/cm^3)	ρ_{env} (g/cm^3)	ε (%)
3 %SF	1.32 ± 0.06^{a*}	0.10 ± 0.02^{a*}	93 ± 0.02
3 %SF 10:1	1.22 ± 0.05^{b*}	0.10 ± 0.01^{a*}	94 ± 0.01
3 %SF 5:1	1.24 ± 0.03^{b*}	0.07 ± 0.01^{a*}	94 ± 0.01
3 %SF 2:1	1.26 ± 0.10^{b*}	0.07 ± 0.01^{a*}	94 ± 0.01
5 %SF	1.26 ± 0.01$^{a\#}$	0.10 ± 0.02^{a*}	92 ± 0.02
5 %SF 10:1	1.22 ± 0.03^{a*}	0.10 ± 0.01^{a*}	92 ± 0.01
5 %SF 5:1	1.31 ± 0.04$^{b\#}$	0.11 ± 0.03^{a*}	91 ± 0.03
5 %SF 2:1	1.29 ± 0.02^{a*}	0.09 ± 0.01^{a*}	93 ± 0.01
7 %SF	1.31 ± 0.04$^{a*\#}$	0.11 ± 0.02^{a*}	92 ± 0.02
7 %SF 10:1	1.22 ± 0.05^{b*}	0.08 ± 0.01^{a*}	93 ± 0.01
7 %SF 5:1	1.27 ± 0.05$^{a*\#}$	0.09 ± 0.02^{a*}	93 ± 0.02
7 %SF 2:1	1.28 ± 0.04^{a*}	0.09 ± 0.01^{a*}	93 ± 0.01

at 91–94 % across formulations.

Table 3 summarizes key insights into the textural properties of ADO-SF microparticles, including specific surface area, pore volume, and pore size distribution. All ADO-SF microparticles formulations exhibit high specific surface areas (191 to 306 m^2/g) and significant pore volumes (0.95–2.65 cm^3/g). The V_{mes} and V_{mac} values are relatively consistent across compositions, ranging from 0.85 to 1.99 cm^3/g and 8.05 to 12.48 cm^3/g, respectively. Although the 5 %SF 2:1 is the formulation that presents lower overall specific pore, mean pore diameter and specific mesopore volume. Macropores contribute over 83 % of the total pore volume across all formulations, indicating that the aerogels have a highly interconnected, open structure. This architecture is expected to enhance the loading capacity of bioactive agents and facilitate the diffusion of nutrients and oxygen when applied to wound sites

Table 3
Textural properties evaluated by nitrogen adsorption–desorption test of the ADO-SF microparticles.

Particles	Specific Surface area (m^2/g)	Total specific pore volume (cm^3/g)	Average pore diameter (nm)	V_{mes} (cm^3/g)	V_{mac} (cm^3/g)
3 %SF	211 ± 11	1.62 ± 0.08	25.69 ± 1.28	1.23 ± 0.06	9.66 ± 2.69
3 %SF 10:1	290 ± 14	2.34 ± 0.12	26.88 ± 1.34	1.87 ± 0.09	8.60 ± 0.74
3 %SF 5:1	306 ± 15	2.65 ± 0.13	28.77 ± 1.44	1.99 ± 0.10	11.97 ± 1.71
3 %SF 2:1	193 ± 10	1.76 ± 0.09	29.51 ± 1.48	1.31 ± 0.07	12.48 ± 1.44
5 %SF	243 ± 12	2.07 ± 0.10	28.15 ± 1.41	1.59 ± 0.08	9.08 ± 1.93
5 %SF 10:1	231 ± 12	1.85 ± 0.09	26.41 ± 1.32	1.47 ± 0.07	8.21 ± 1.02
5 %SF 5:1	191 ± 10	1.38 ± 0.07	23.20 ± 1.16	1.11 ± 0.06	8.17 ± 2.13
5 %SF 2:1	207 ± 10	0.95 ± 0.05	15.97 ± 0.80	0.85 ± 0.04	10.85 ± 1.47
7 %SF	229 ± 11	1.82 ± 0.09	26.06 ± 1.30	1.52 ± 0.08	8.05 ± 2.13
7 %SF 10:1	217 ± 11	1.72 ± 0.09	26.09 ± 1.30	1.31 ± 0.07	11.16 ± 1.74
7 %SF 5:1	217 ± 11	1.86 ± 0.09	28.04 ± 1.40	1.49 ± 0.07	9.87 ± 2.67
7 %SF 2:1	232 ± 12	1.87 ± 0.09	26.76 ± 1.34	1.47 ± 0.07	9.57 ± 1.33

(Bernardes et al., 2021; Athamneh et al., 2023).

Although increasing ADO content generally correlates with higher surface area and pore volume, the relationship between ADO concentration and textural properties does not show a clear linear trend across all formulations. For instance, while 3 % SF formulations with lower ADO ratios (10:1 and 5:1) exhibit increased surface area and mesopore volume, 5 % and 7 % SF formulations do not follow this trend consistently. The absence of directional influence at higher SF concentrations suggests that the SF matrix reaches structural saturation, where further increases have minimal impact on the overall structure and ADO's effect on the porous network.

The chemical structure of the ADO-SF microparticles was investigated by FTIR-ATR analysis (Fig. 3A).

The obtained spectra confirmed the presence of the main characteristic bands of SF, attributed to the β-sheet conformation, with strong bands in the amide I and amide II regions (Bernardes et al., 2023). This structure will confer to the aerogel particles robust mechanical properties and biological performance (Hu et al., 2012). The integrity of SF was maintained after the addition of ADO. DSC analysis was performed to evaluate the thermal stability and behaviour of ADO-SF microparticles in comparison to pure ADO (Fig. 3B). The DSC thermogram for pure ADO (Fig. 3B.a) displays a distinct and sharp endothermic peak at approximately 237 °C, which corresponds to the melting temperature of

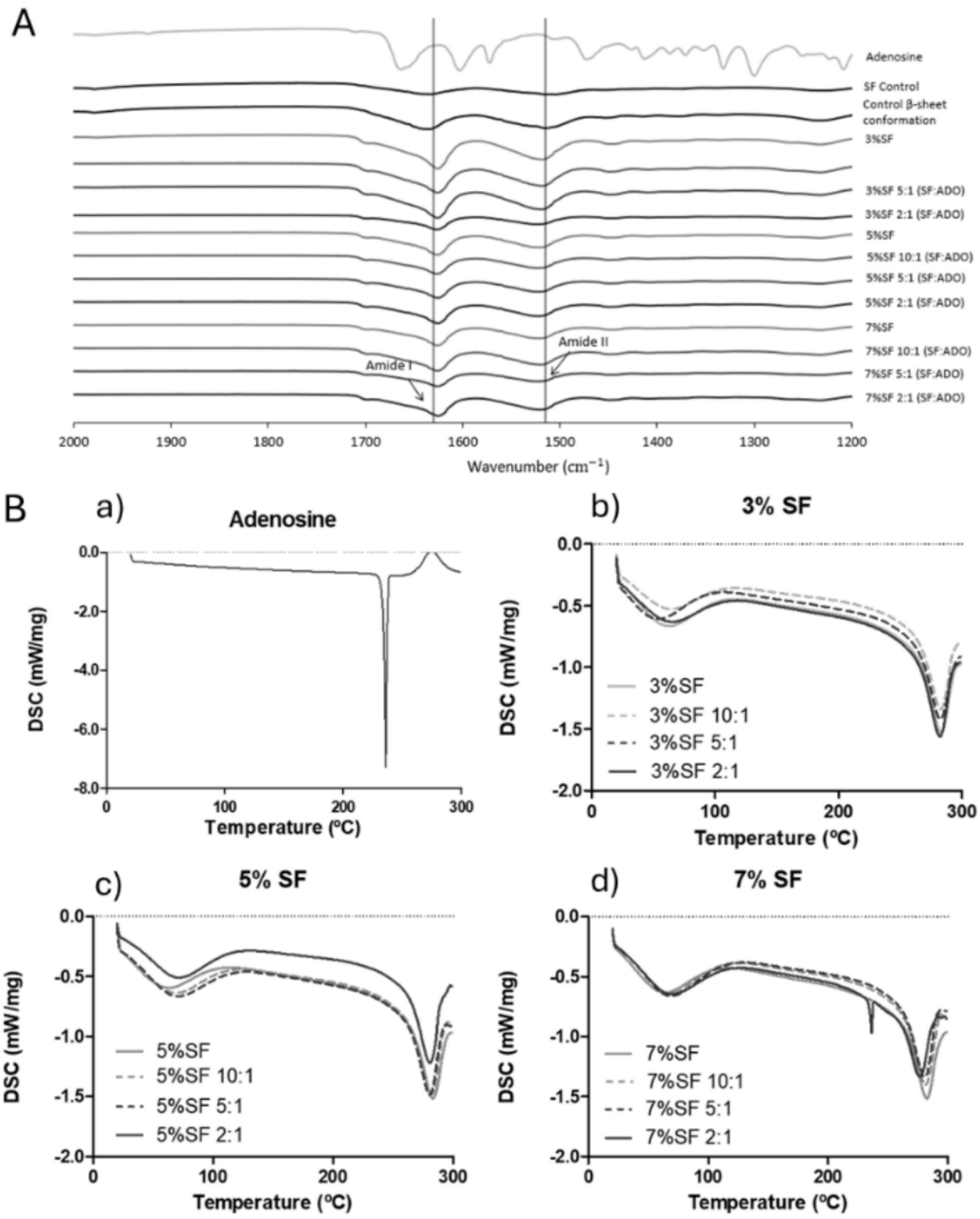

Fig. 3. A. FTIR-ATR spectra of ADO-SF microparticles with 3%, 5% and 7% SF (w/v) without and with a ratio of SF:ADO (wt:wt) of 10:1, 5:1, 2:1; and SF controls: SF without and with β-sheet conformation; B. DSC analysis of a) ADO pure powder, b) 3%SF, c) 5%SF and d) 7% SF aerogel particles for each ADO concentration.

ADO (Hoyer and Barrett, 1966). This peak is indicative of the crystalline structure of ADO, thereby demonstrating a high degree of purity and stability in the unprocessed form. The DSC thermograms of ADO-SF microparticles (Fig. 3B.b-d) show broad endothermic transitions between 50–80 °C related to the loss of bound water or dehydration of the SF component, along with a sharp endothermic peak at 220–240 °C associated with the thermal degradation or structural transitions of SF across all samples, regardless of SF concentration. From all the analysed samples, the presence of ADO was only detected for 7 % SF samples, which incorporated the highest amount of ADO (2:1 ratio). This formulation exhibits an endothermic peak around 237 °C, which matches the melting behavior of pure ADO.

3.2. ADO quantification, loss analysis, and release from ADO-SF microparticles

The ADO concentration, loading capacity, and entrapment yield of the ADO-SF microparticles were assessed to evaluate the encapsulation efficiency and the potential for controlled drug release (Table 4). Higher SF concentrations, particularly the 7 % SF formulations, exhibited relatively improved ADO loading and entrapment yield compared to lower concentrations. However, the overall values for drug loading and entrapment yield were low, highlighting inefficiencies in the encapsulation process. To address these inefficiencies, the loss of ADO during centrifugation was investigated, revealing that over 67 % of ADO was lost during this step, contributing significantly to the reduced encapsulation efficiency.

The release profiles for different ADO-SF microparticles (Fig. 4) had a significant initial burst release of ADO within the first 15 min, during which ca. 50–60 % of the loaded ADO was released. This burst release is attributed to the rapid diffusion of ADO from the surface and near-surface regions of the SF aerogel matrix into the surrounding medium. After this initial phase, a plateau is reached within about 1 h, with no sample achieving complete (100 %) ADO release. The data showed different release patterns for each SF concentration group. In the 3 % SF formulations, the 10:1 ratio released faster than the 5:1 and 2:1 ratios, probably due to reduced matrix saturation, which favours faster diffusion. This formulation also had a higher shell density and porosity, which increased the release rate. Conversely, the 7 % SF group showed slower sustained release at the 2:1 ratio, which had the highest specific surface area and pore volume. This trend is likely to be due to increased SF density or stronger ADO-SF interactions resulting in more controlled release. Some ADO may also precipitate in the matrix, inhibiting dissolution. The 5 % SF formulations showed consistent release at all ratios, indicating stable release regardless of ADO loading.

3.3. In vitro cell studies

3.3.1. ADO

ADO plays a crucial role in cellular signalling and inflammation regulation. Having this into consideration the effect of ADO on the viability of HDF, HaCaT, and HDMEC cells was assessed at different concentrations (Fig. 5) as first screening to identify the best concentration levels to be delivered to cells.

As shown in Fig. 5, cytocompatibility varies with cell type. HDF cells (Fig. 5A) presented a cell viability in the order of 100 % or higher for all the tested concentrations, with a tendency for its increase with decreasing ADO concentration. HaCaT (Fig. 5B) cells exhibited cytocompatibility at lower concentrations (0.1 and 0.2 mg/ml). However, at concentrations above 0.45 mg/ml, ADO became cytotoxic to these cell types, showing significant sensitivity. This suggests that HDF cells are highly resilient to ADO, even at elevated doses, whereas HaCaT and HDMEC cells are more prone to cytotoxic effects at higher concentrations.

3.3.2. ADO-SF particles

The resazurin assay was used to evaluate the cytocompatibility of the different developed ADO-SF formulations over 7 days, with cell viability percentages serving as indicators of potential cytotoxicity (Fig. 6).

Fig. 6A demonstrates that all the tested ADO-SF microparticle formulations are cytocompatibility towards HDF cells, maintaining the average viability levels above 100 %. Significant differences are observed between the control (cells with no particles) and the ADO-SF microparticles with concentrations of 3 % SF 2:1, 5 % SF 5:1 and 2:1, and 7 % SF 10:1 and 5:1 at Day 1. This suggests that formulations with higher ADO concentrations exhibit the best cell viability, as expected, based on the results obtained at Fig. 5. However, no significant differences are evident between these groups and the control group on Days 3 and 7.

The HaCaT cells (Fig. 6B) exhibited enhanced cell viability, exceeding 100 % compared to the control over the seven-day observation period. On Day 1, statistically significant differences were observed between the 5 % SF, 5 % SF 10:1, 7 % SF, and 7 % SF 2:1 groups, with all groups showing a significant reduction compared to the control. In this case, no dose-dependent relationship with ADO concentration was observed. By day 3, the cell viability of the ADO-SF microparticles increases, reaching a value above 100 %. Notably, the 3 % SF 10:1 and 7 % SF formulations also significantly enhanced cell viability.

HDMEC cells (Fig. 6C) were the most sensitive of the three cell types, displaying significant viability reductions in response to higher concentrations and extended exposure. Significant differences were noted in multiple samples as early as day 1, (3 % SF 2:1, 5 % SF 2:1, 7 % SF and 7 % SF 2:1) showing that HDMEC cells present cytotoxicity with the formulation with higher ADO concentration. By Day 3, only 5 % SF 10:1, 5 % SF 5:1, and 7 % SF 5:1 did not show significant differences. However, all formulations with higher ADO concentrations (2:1) exhibited cytotoxic effects by this time. By Day 7, all samples exhibited cytotoxicity compared to the cell control. However, this effect could potentially be attributed to the limited adaptation of these cells to direct contact with the aerogel particles over time, along with their restricted ability to migrate, which may have influenced the results.

Fig. 7 provides insights into the effects of ADO-SF microparticles on the proliferation of HDF, HaCaT and HDMEC cells.

HDMEC showed a significant decrease in proliferation over time in

Table 4
ADO concentration, loading efficiency, and entrapment yield for ADO-SF microparticles.

Particles	ADO concentration (μg/ml)	Loading (%)	Entrapment Yield (%)	Mass of ADO lost during centrifugation (mg)	ADO loss during Centrifugation / Total Mass Added (%)
3 %SF 10:1	0.40 ± 0.16	0.06 ± 0.02	0.57 ± 0.23	34.76 ± 4.02	77.25 ± 8.93
3 %SF 5:1	1.75 ± 0.26	0.25 ± 0.04	1.26 ± 0.19	70.17 ± 4.02	77.97 ± 4.47
3 %SF 2:1	3.28 ± 0.56	0.47 ± 0.08	0.95 ± 0.16	175.74 ± 5.58	78.11 ± 2.48
5 %SF 10:1	1.44 ± 0.22	0.21 ± 0.03	2.07 ± 0.32	53.17 ± 1.05	70.89 ± 1.40
5 %SF 5:1	3.77 ± 0.34	0.54 ± 0.05	2.72 ± 0.24	115.40 ± 2.77	76.96 ± 1.85
5 %SF 2:1	5.96 ± 0.23	0.86 ± 0.03	1.72 ± 0.07	290.08 ± 7.81	77.35 ± 2.08
7 %SF 10:1	2.51 ± 0.42	0.36 ± 0.06	3.63 ± 0.61	70.55 ± 1.20	67.19 ± 1.14
7 %SF 5:1	5.84 ± 1.11	0.84 ± 0.16	4.21 ± 0.80	141.10 ± 2.02	67.19 ± 5.72
7 %SF 2:1	64.29 ± 7.71	9.28 ± 1.11	18.56 ± 2.22	348.50 ± 9.00	66.38 ± 1.71

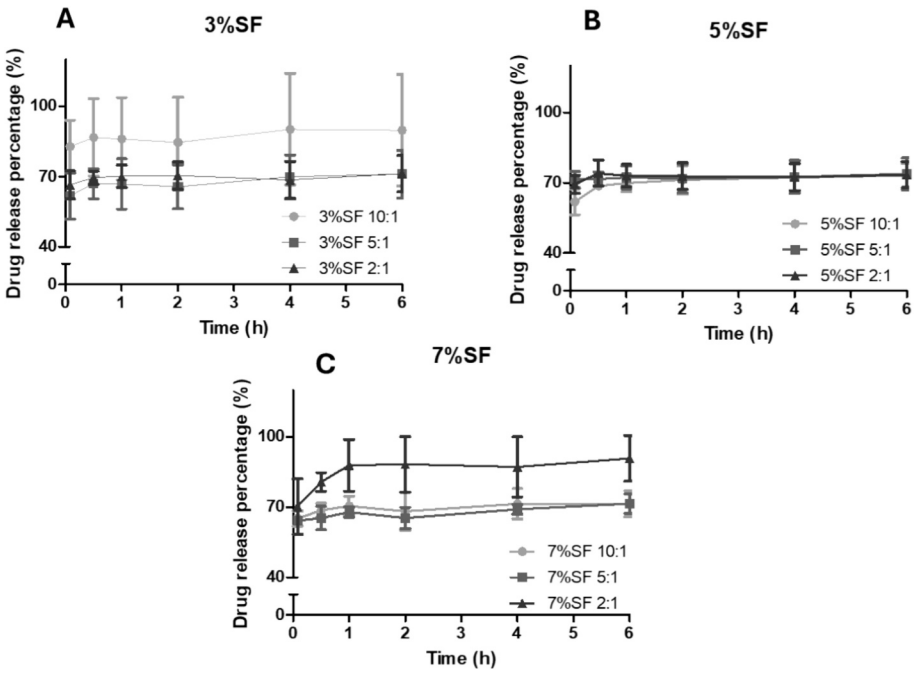

Fig. 4. Drug release profile of ADO from formulated microparticles with different ADO:SF ratios (10:1; 5:1 and 2:1) using (A) 3 %, (B) 5 % and (C) 7 % SF aerogel microparticles (37 °C, 100 rpm, PBS pH 7.4).

response to ADO-SF microparticles exposure, whereas no significant differences were observed in HDF and HaCaT cells compared to controls.

For HDF cells (Fig. 7A), no significant differences were observed between the control and ADO-SF microparticles-treated groups by Day 7. However, there were significant reductions in proliferation at day 3, observed with particles without ADO and 7 % SF 10:1 particles. In HaCaT cells (Fig. 7B), no significant differences in proliferation were observed between the control and ADO-SF microparticles groups at any time point. HDMEC cells (Fig. 7C) had good initial viability and proliferation within 24 h of stimulation with ADO-SF microparticles. While initial cell proliferation was observed in HDMECs within the first 3 days of ADO-SF microparticles exposure, a significant reduction in cell viability and proliferation was evident by Day 7. Given the sensitivity of endothelial cells, the particles may form a layer that influences cellular behaviour, potentially affecting the proliferation process. This effect may be especially relevant when working with cell types that are inherently sensitive to changes in their microenvironment.

3.3.3. *Cell morphology*

The SEM images (Fig. 8A) provide a detailed visualization of the interaction between the cells and the ADO-SF microparticles over time. Representative images were selected based on previous results, with particular focus on the 5 % SF and 5 % SF 5:1 formulations, which were considered representative due to their consistent performance. The images show strong attachment of the aerogel particles to cell surfaces after washing, indicating favorable interaction between the cells and ADO-SF microparticles. It suggests the effective cell-particle integration, which is important for applications in tissue regeneration or drug delivery, as it demonstrates the ability of the aerogel particles to maintain close contact with cells, promoting potential therapeutic effects. Fluorescence micrographs (Fig. 8B) demonstrate successful cell proliferation over time. Early images show scattered cells, while later images depict a densely packed monolayer. This progression, visible in both fluorescence and SEM images, indicates a favourable culture environment and robust cell growth. The green fluorescence reveals the actin cytoskeleton, indicating strong cell attachment and spreading. Over time, the actin network becomes more interconnected, signifying enhanced cell communication and healthy structural development. The blue fluorescence highlights the nuclei, suggesting uniform proliferation without clustering. Additional details can be found in the Supplementary Information, including SEM and fluorescence microscopy images of HDF, HaCaT keratinocytes, and HDMEC at days 1, 3, and 7, illustrating cell-material interactions.

4. Discussion

4.1. *ADO-SF microparticles properties*

Given the pivotal role of ADO in wound healing, a comprehensive evaluation of the ADO-SF particles reveals their promising potential for such applications, based on their textural, morphological, and chemical attributes. The aerogel particles present a highly porous structure with an interconnected network of well-defined pores. The observed high porosity and specific surface area of all ADO-SF microparticles formulations reinforce their suitability for use in drug delivery systems. The interconnected pore structure facilitates not only controlled drug release but also supports cell migration and tissue integration, which are both critical elements of the wound healing cascade (Jeong et al., 2024). Moreover, the uniformity of the macropore volume across varying ADO concentrations indicates structural stability within the aerogel matrix despite ADO incorporation. The ADO-SF microparticles exhibit a high specific surface area and substantial pore volume, comparable to other reported SF-based aerogels (Bernardes et al., 2023; Marin et al., 2014; Mallepally et al., 2015). This finding supports the notion that the porous architecture of the SF matrix is preserved, even after ADO integration. Following the IUPAC classification, the ADO-SF microparticles display type IV isotherms, which are indicative of mesoporous materials with interconnected pore networks. The pore sizes, which predominantly range from 15 to 30 nm, fall within the mesoporous regime, which is optimal for sustained and controlled release applications (López-Iglesias et al., 2019; Horvat et al., 2022; Naito et al., 2018). Such mesoporous features provide effective diffusion channels, ensuring prolonged and efficient drug release. Furthermore, DSC analysis indicates that ADO remains stable within the SF matrix. The broad endothermic peaks from SF dehydration and structural relaxation suggest the formation of stable, hydrated aerogel structures, which are beneficial for drug release.

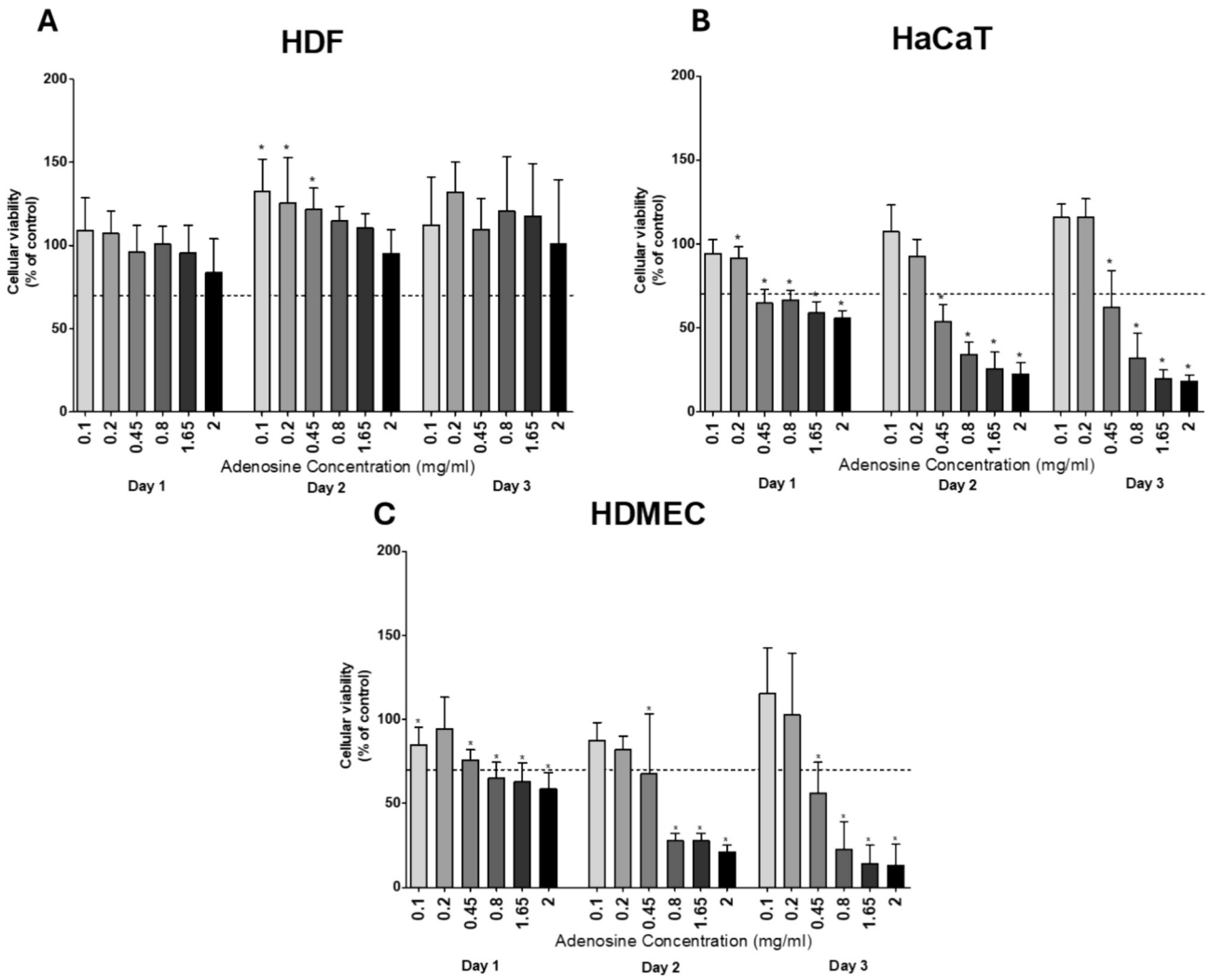

Fig. 5. Cell viability after MTT assay of a control group and cells cultured with ADO at different concentrations (0.1–2 mg/mL) of A) HDF, B) HaCaT and C) HDMEC cells ($\alpha < 0.05$). *The differences from each time-point's negative control (cell growth) were significant at $p < 0.05$.

Chemical analysis demonstrated that the integrity of SF is maintained in the presence of ADO, indicating chemical compatibility between these components.

4.2. Drug quantification and release of ADO-SF microparticles

The synthesis of ADO-SF microparticles was conducted using a methodology that involved two centrifugation steps, followed by supercritical CO_2 drying. The choice of this drying method allowed to preserve the integrity of the particles to create the aerogel structure while minimizing ADO loss during solvent exchange due to its poor solubility in ethanol. Still, this was only partially achieved due to the water present initially in the particles. As a consequence, some of the ADO was co-eliminated removed along with water during the solvent exchange, which resulted in a reduction in the encapsulation efficiency and a decrease in both drug loading and entrapment yield. Notably, most of the ADO loss occurred during the first centrifugation step, while the second centrifugation resulted in minimal to no additional loss, which highlights the need for further optimization of the solvent exchange and drying process in order to minimise ADO leaching. It is possible that alternative methods or modified conditions in the centrifugation or solvent exchange steps could enhance ADO retention within the SF matrix. Enhancing encapsulation efficiency may involve refining centrifugation parameters, adjusting solvent exchange protocols, or implementing alternative approaches that leverage stronger hydrophilic or hydrophobic interactions to stabilize ADO. The use of surfactants or stabilizers, such as polysorbates (synthetic non-ionic surfactants) or cyclodextrins, could further enhance ADO retention, reducing premature drug loss during processing (Jin and Zhang, 2024; Ravichandran et al., 2021). Such improvements are critical for achieving higher drug loading and entrapment yields, thereby enhancing the effectiveness of SF-based systems for controlled release applications.

SF's capacity to form exceptionally stable matrices, coupled with its inherent biocompatibility and ability to create drug-entrapping coatings, positions it as a highly effective material for prolonging drug release and improving the therapeutic outcomes of unstable drugs, including ADO (Pritchard et al., 2010; Tomeh et al., 2019). Previous studies have also investigated the encapsulation of ADO using alternative carriers, providing valuable insights into the challenges associated with its efficient loading. For instance, recognizing the short half-life of ADO in biological environments, nanoparticles of chitosan were explored as potential delivery vehicles (Kazemzadeh-Narbat et al., 2015). These nanoparticles exhibited an encapsulation efficiency of 20 % and a loading capacity of 3 %. The authors attribute these values to the weak positive charge of ADO molecules (approaching neutrality with an isoelectric point near pH 7). Furthermore, the proximity of ADO's isoelectric point to that of chitosan likely limits significant ionic interactions between the two molecules, hindering efficient

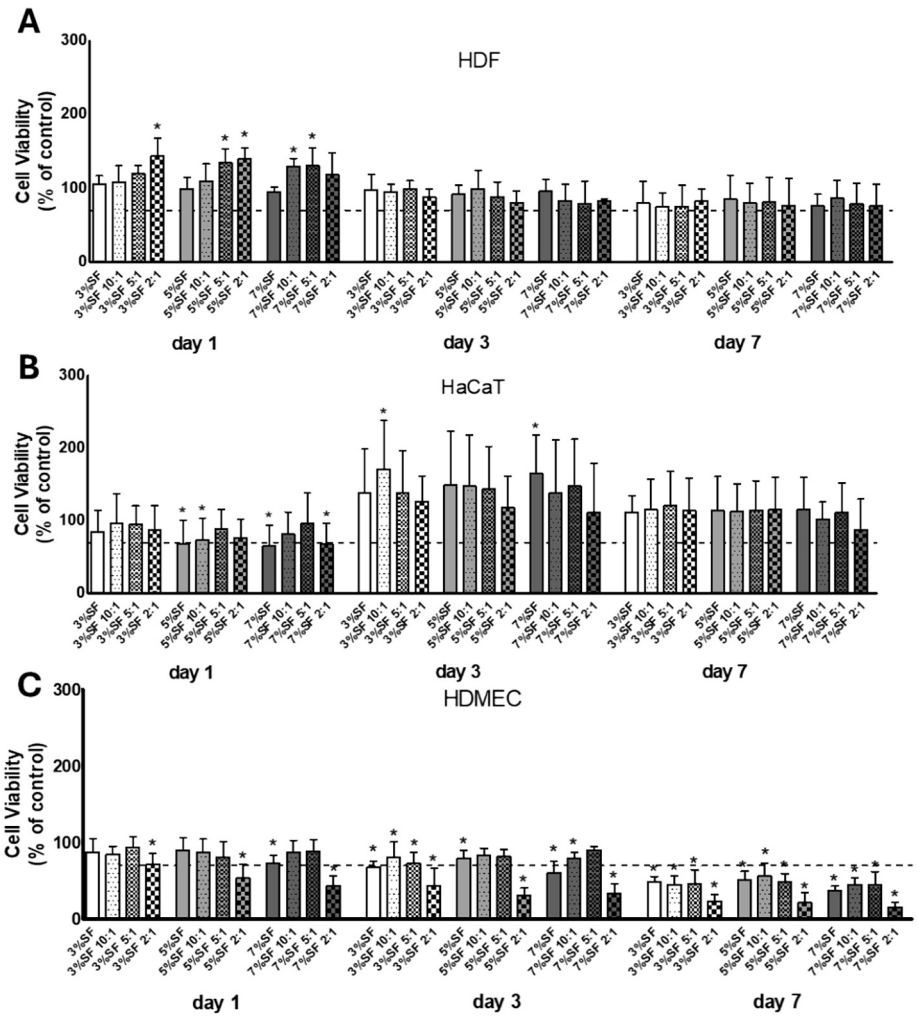

Fig. 6. Cell Viability of A) HDF, B) HaCaT and C) HDMEC after 1, 3 and 7 days in contact with ADO-SF aerogel microparticles. * The differences from the negative control (cell s without materials) of each time-point were significant at $\alpha < 0.05$.

encapsulation (Kazemzadeh-Narbat et al., 2015). Considering the potential ionic interactions between ADO and SF, examining the protein's structure is crucial. SF's heavy chain comprises 12 hydrophobic domains interspersed with 11 smaller hydrophilic ones (Jameson et al., 2021). Within these hydrophobic domains, a repetitive hexapeptide sequence is present, known for its ability to form stable anti-parallel β-sheet crystalline structures (Bernardes et al., 2023). ADO is a nonpolar molecule with some hydrophobic regions within its structure. ADO, while primarily hydrophilic, engages in significant hydrophobic interactions, particularly in the context of receptor binding and enzyme inhibition (Gomes Daré et al., 2024; Van Galen et al., 1990; Kim et al., 2003). These interactions are crucial for its biological functions and potential therapeutic applications. The exploration of ADO's hydrophobic regions continues to be an area of interest for developing new pharmacological agents. These hydrophobic regions can interact weakly with the hydrophobic domains of SF, which are rich in nonpolar amino acids like alanine and glycine.

Daré et al. (2024) improved ADO association efficiency (AE) in nanostructured lipid carriers (NLCs) by exploiting hydrophilicity. They found that replacing the hydrophobic Miglyol 810 N with the more hydrophilic Capmul MCM C-8 significantly enhanced ADO incorporation, raising AE from 5.73-13.8 %, likely due to improved interactions between the hydrophilic drug and carrier (Gomes Daré et al., 2024).

An initial rapid release of ADO was observed, which is attributed to the rapid diffusion of the drug from the surface and near-surface regions of the SF aerogel matrix into the surrounding solution. This rapid release is particularly advantageous given the extremely short half-life of ADO *in vivo* (Kazemzadeh-Narbat et al., 2015). By delivering ADO promptly to the target site, the burst release helps to overcome this pharmacokinetic limitation. This enables the immediate activation of biological responses, such as anti-inflammatory effects, and the initiation of cellular signalling pathways that are critical for wound healing and tissue regeneration (Bernardes et al., 2021). Subsequently, a plateau was reached within approximately one hour, with none of the samples achieving 100 % ADO release. These release results indicate that a proportion of the ADO was retained within the SF matrix, presumably due to interactions between the drug and the SF structure or its entrapment within less accessible regions of the aerogel. A similar drug release pattern was observed, with a chitosan nanoparticulate system incorporating ADO exhibiting an initial burst release of approximately 42 % within the first hour, followed by a very slow release of around 5 %, reaching nearly a plateau (Kazemzadeh-Narbat et al., 2015). Pritchard et al. (Pritchard et al., 2010), investigated the use of SF coatings to achieve controlled, sustained release of ADO from solid powder reservoirs. Release was modulated by the number of SF layers, created through repeated dipping of powder in silk solution. By precisely controlling the silk coating, this study achieved linear, sustained release of ADO for up to 17 days from encapsulated reservoirs coated with eight layers of SF (8 % w/v) (Pritchard et al., 2010). Studies in the UK and Denmark show that dressings are typically changed about three times

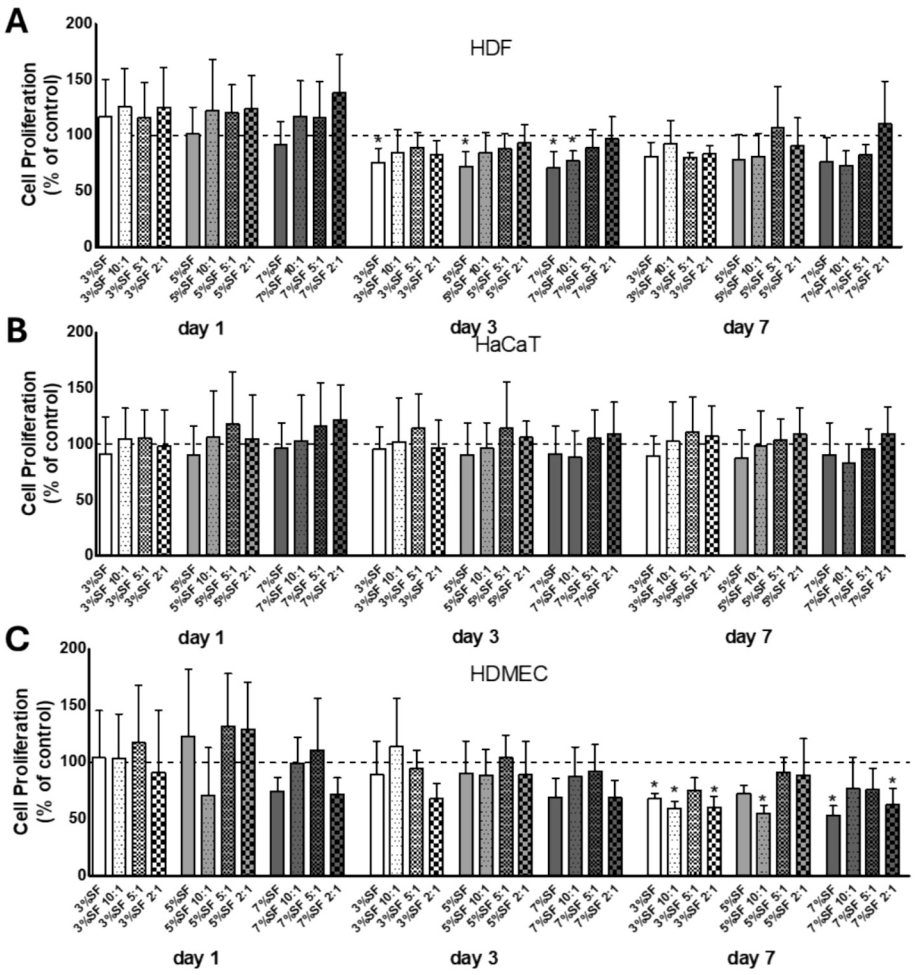

Fig. 7. Cell Proliferation of A) HDF, B) HaCaT and C) HDMEC after 1, 3 and 7 days in contact with ADO-SF aerogel microparticles. * The differences from the negative control (cell growth) of each time-point were significant at $\alpha < 0.05$.

per week, with 23 % of wounds requiring daily changes (Lindholm and Searle, 2016). Dressing frequency should be tailored to the patient and wound, as unnecessary changes can impact patient well-being and healthcare resources (Lindholm and Searle, 2016). Since chronic inflammatory wounds often require dressing changes every 3–4 days, a sustained release of ADO over at least three days would be beneficial. Despite ADO loss, the developed particles maintained cytocompatibility and cell proliferation, with released ADO remaining within its therapeutic window for the lowest ratio. As part of future efforts, the addition of an external protective layer was considered to regulate drug release kinetics and improve the retention and sustained delivery of ADO.

4.3. *In vitro behaviour of ADO-SF microparticles*

Considering the *in vitro* results, the viability of cells exposed to particles without ADO was lower compared to the formulations containing ADO at 5:1 and 10:1 wt ratios. Samples with an ADO weight ratio of 2:1 exhibited reduced cell viability in HaCaT and HDMEC cells, which are more susceptible to cytotoxic effects at higher ADO concentrations, as indicated by conditioned medium results. The presence of ADO significantly improved cell viability compared to formulations lacking ADO. A similar trend was observed in proliferation assays; however, at a 2:1 ratio, HDF and HaCaT cells demonstrated enhanced proliferation, suggesting that ADO may also promote cell proliferation. Notably, in HDMEC cells, the 5 % SF 5:1 formulation exhibited the highest proliferation rates over the tested period.

The *in vitro* cytocompatibility assays conducted in this study indicate that in general ADO enhances cell viability in a dose-dependent manner, particularly in case of HDF cells, thereby supporting its potential use in dermal regeneration. However, the HaCaT and HDMEC cells displayed increased sensitivity to ADO, with toxicity manifesting at higher concentrations. The obtained results are consistent with the findings of Daré et al., who investigated the cytotoxicity of free ADO (0.4–800 μg/mL) on NIH-3 T3 fibroblasts and HaCaT cells (Gomes Daré et al., 2024). Furthermore, they examined the impact of free ADO cell proliferation. Notably, their data revealed that NIH-3 T3 and HaCaT cells maintained proliferation within the ADO concentration range of 0.8 to 12.5 μg/mL (Gomes Daré et al., 2024). Precise ADO concentration is essential for safe and effective wound healing, requiring a balance between fibroblast activation and keratinocyte/endothelial viability, given their distinct roles in skin structure and repair. The specific contributions of these cell types across different skin layers and wound repair stages highlights the necessity for careful concentration regulation in formulation development. This is exemplified by a study on controlled drug release patches for wound healing, which enable precise dosing to maintain therapeutic drug levels (Hassan et al., 2021). These patches promote efficient wound repair and proper progression through healing phases, as demonstrated by *in vitro* and *in vivo* evaluations confirming their effectiveness in accelerating healing and highlighting the importance of concentration control in wound care applications.

For HDF, ADO is known to stimulate collagen production in dermal fibroblasts through A_{2A} receptors and promotes the synthesis of factors such as IL-13 and connective tissue growth factor, thereby enhancing collagen synthesis (Chen et al., 2024). Perez-Aso et al., (Perez-Aso et al.,

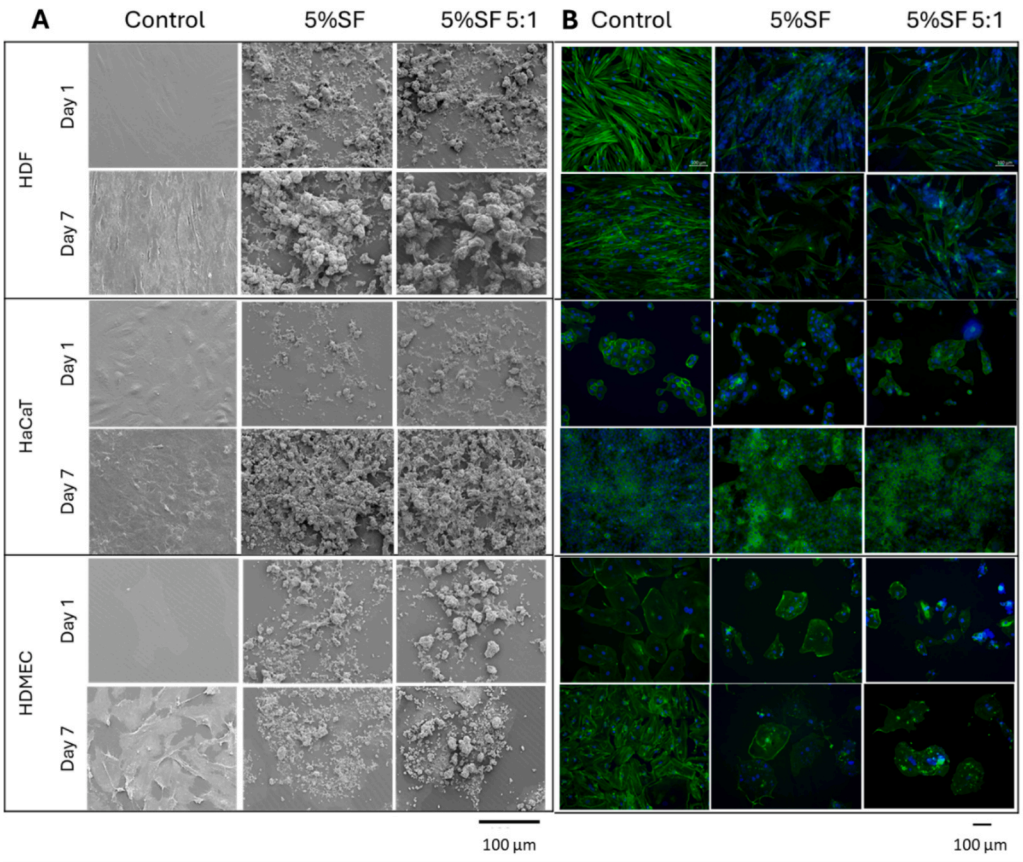

Fig. 8. Cell morphology of HDF, HaCaT and HDMEC after 1 and 7 day in contact with aerogels: (A) SEM and (B) fluorescence (with nuclei stained blue and the cytoskeleton stained green) microscopies images of control, 5 % SF and 5 % SF 5:1 samples.

2014) studied how the A_{2A} receptor promotes collagen production in human fibroblasts and concluded that the A_{2A} receptor activates two pathways (cyclic AMP and AKT) in cells, leading to increased collagen production, which is crucial for wound healing. The cyclic AMP pathway is a signaling pathway that is involved in many cellular processes, including cell growth and differentiation. The AKT pathway is a signaling pathway that is involved in cell survival and proliferation (Perez-Aso et al., 2014). In the case of HaCaT cells, a trend was observed wherein increased ADO loading in the SF aerogel particles corresponded with a decrease in cell viability. Nevertheless, cell viability remained above the control on Day 1, indicating that ADO's interaction with HaCaT receptors may contribute to this initial effect. ADO has complex receptor-specific effects on keratinocytes, capable of both pro-inflammatory and anti-inflammatory actions depending on the receptor subtype expressed. Previous studies have shown that ADO inhibits keratinocyte proliferation via A_{2B} receptors while promoting proliferation via A_{2A} receptors (Chen et al., 2024; Andrés et al., 2017). In inflammatory conditions, altered receptor expression can influence keratinocyte responses, which is significant in the context of pathological epidermal hyperplasia. Based on the obtained results, the presence of ADO in the ADO-SF formulations enhances proliferation behavior, suggesting the activation of A_{2A} receptors, which may support wound healing by promoting keratinocyte proliferation and re-epithelialization. NLCs loaded with simvastatin and 2 % ADO was studied to understand how the concentration of NLCs affects the cell viability (Gomes Daré et al., 2024). NIH-3T3 fibroblasts and HaCaT keratinocytes were treated with two ratios of simvastatin and ADO incorporated in the nanostructured lipid carrier. They conclude that simvastatin influences the NLC's cell viability, independently of the amount of ADO.

HDMECs exhibited pronounced sensitivity to ADO-SF microparticles, particularly at elevated ADO concentrations. This heightened sensitivity may impede angiogenesis and vascularization processes essential for effective wound healing. *In vivo*, ADO promotes blood vessel growth by attracting early endothelial progenitor cells to the injury site. It also increases the release of Small Extracellular Vesicles from these cells, further stimulating blood vessel formation and cell proliferation (~50 %) (Oporto et al., 2023). The dose-dependent cytotoxic effect of ADO was apparent across different cell types, with notably higher cytotoxicity observed in HDMECs. The observed cytotoxicity may not be solely due to the concentration of ADO, but may also be due to the formation of a layer of ADO-SF microparticles on the cell surface, potentially leading to cell suffocation. Given the increased susceptibility of HDMECs, the presence of this deposited layer likely exacerbates cell viability issues, contributing significantly to the cytotoxic effects, especially by day 7. A similar trend was observed in cell proliferation assays. Notably, only the 5 % SF 5:1 and 5 % SF 2:1 formulations exhibited no significant differences in proliferation by day 7, indicating that these specific formulations hold promise for further development. Therefore, formulations aimed at targeting endothelial cells must employ low concentrations of ADO to minimize cytotoxicity and maintain the cells' pro-angiogenic capabilities. SEM analysis showed HDF and HaCaT cells distributed throughout the aerogel particles, indicating interaction. In contrast, HDMEC cells were primarily located at the bottom of the particles, suggesting a lack of integration. Overall, ADO demonstrated varying effects on different cell types. While it promoted fibroblast activity, enhancing collagen production, it exhibited a dose-dependent cytotoxic effect on keratinocytes and endothelial cells. Given the available literature in the field and the present results, precise concentration control of ADO in topical formulations is crucial for effective wound healing, as the optimal dosage depends on both wound depth and the specific cell types present in each skin layer, such as keratinocytes in the epidermis and

fibroblasts and endothelial cells in the dermis (Bernardes et al., 2021).

5. Conclusions

This study highlights the potential of ADO-loaded SF microparticles as promising candidates. Through comprehensive physicochemical characterization, the aerogel particles demonstrate high porosity, structural stability and mesoporosity. Despite partial loss of ADO during processing, particularly in the solvent exchange phase, the synthesis approach developed maintained a balance between particle integrity and drug retention. ADO incorporation increased the cell proliferation and viability of HDF, HaCaT and HDMEC on day 1. However, dose-dependent cytotoxic effects were observed in HaCaT and HDMEC, highlighting the need and the importance of fine-tunning ADO dosage and release kinetics. While ADO can stimulate HDF activity, its excessive release may negatively impact HaCaT and HDMEC cells.

The developed SF aerogel microparticles possess key attributes, such as high porosity, biocompatibility, and the capacity to support cell proliferation, that support their potential for localized drug delivery in tissue regeneration contexts. Nonetheless, this study is limited to *in vitro* findings; thus, no definitive conclusions regarding wound healing efficacy can be drawn at this stage. Future work should focus on *in vivo* evaluation of ADO-SF formulations to determine their therapeutic performance relative to current wound healing treatments, including other silk-based materials. Furthermore, as ADO was used here as a model drug, this platform could be adapted for the delivery of other sensitive bioactive molecules, broadening its relevance in regenerative medicine.

CRediT authorship contribution statement

Beatriz G. Bernardes: Writing – review & editing, Methodology, Conceptualization, Visualization, Formal analysis, Validation, Writing – original draft, Investigation, Data curation. **Rossella Laurano:** Methodology, Investigation, Writing – review & editing. **Clara López-Iglesias:** Methodology, Investigation, Writing – review & editing. **Rui Magalhães:** Investigation, Writing – review & editing. **Raquel Costa:** Supervision, Methodology, Conceptualization, Writing – review & editing. **Carlos A. García-González:** Supervision, Resources, Writing – review & editing, Funding acquisition, Conceptualization. **Ana Leite Oliveira:** Conceptualization, Writing – review & editing, Resources, Funding acquisition, Supervision.

Declaration of competing interest

The authors declare that they have no known competing financial interests or personal relationships that could have appeared to influence the work reported in this paper.

Acknowledgements

This work was supported by National Funds from Fundação para a Ciência e a Tecnologia (FCT), through project UIDB/50016/2020, Doctoral Research Grant 2021.05717.BD (DOI: 10.54499/2021.05717.BD). Work supported by IBEROS+ (0072_IBEROS_MAIS_1_E) - Instituto de Biofabricación en Red para El Envejecimiento Saludable, funded by "Interreg VI A España – Portugal (POCTEP) 2021-2027"; by MICINN [PID2023-151340OB-I00/AEI/10.13039/501100011033], Agencia Estatal de Investigación [AEI] and FEDER funds. This publication is based on work from ECO-AERoGELS Innovators Grant (ref. IG18125) supported by COST (European Cooperation in Science and Technology). C.L.-I. acknowledges Xunta de Galicia for a postdoctoral fellowship [ED481B-2021-008]. R.L. acknowledges financial support from the FSE REACT-EU - PON Ricerca e Innovazione 2014-2020.

Appendix A. Supplementary data

Supplementary data to this article can be found online at https://doi.org/10.1016/j.ijpharm.2025.125930.

Data availability

Data will be made available on request.

References

Andrés, R.M., Terencio, M.C., Arasa, J., Payá, M., Valcuende-Cavero, F., Navalón, P., Montesinos, M.C., 2017. Adenosine A2A and A2B receptors differentially modulate keratinocyte proliferation: possible deregulation in psoriatic epidermis. J. Invest. Dermatol. 137, 123–131. https://doi.org/10.1016/j.jid.2016.07.028.

Athamneh, T., Hajnal, A., Al-Najjar, M.A.A., Alshweiat, A., Obaidat, R., Awad, A.A., Al-Alwany, R., Keitel, J., Wu, D., Kieserling, H., Rohn, S., Keil, C., Gurikov, P., 2023. In vivo tests of a novel wound dressing based on agar aerogel. Int. J. Biol. Macromol. 239, 124238. https://doi.org/10.1016/j.ijbiomac.2023.124238.

Bernardes, B.G., Del Gaudio, P., Alves, P., Costa, R., García-Gonzaléz, C.A., Oliveira, A.L., 2021. Bioaerogels: promising nanostructured materials in fluid management. Healing Regenerat. Wounds, Mol. 26, 3834. https://doi.org/10.3390/molecules26133834.

Bernardes, B.G., Baptista-Silva, S., Illanes-Bordomás, C., Magalhães, R., Dias, J.R., Alves, N.M.F., Costa, R., García-González, C.A., Oliveira, A.L., 2023. Expanding the potential of self-assembled silk fibroin as aerogel particles for tissue regeneration. Pharmaceutics 15, 2605. https://doi.org/10.3390/pharmaceutics15112605.

Bernardes, B.G., Veiga, A., Barros, J., García-González, C.A., Oliveira, A.L., 2024. Sustainable silk-based particulate systems for the controlled release of pharmaceuticals and bioactive agents in wound healing and skin regeneration. Int. J. Mol. Sci. 25, 3133. https://doi.org/10.3390/ijms25063133.

Borges, P.A., Waclawiak, I., Georgii, J.L., Fraga-Junior, V. da S., Barros, J.F., Lemos, F.S., Russo-Abrahão, T., Saraiva, E.M., Takiya, C.M., Coutinho-Silva, R., Penido, C., Mermelstein, C., Meyer-Fernandes, J.R., Canto, F.B., Neves, J.S., Melo, P.A., Canetti, C., Benjamim, C.F., 2021. Adenosine diphosphate improves wound healing in diabetic mice through P2Y12 receptor activation. Front. Immunol. 12. https://doi.org/10.3389/fimmu.2021.651740.

Chen, L., Lei, X., Mahnke, K., 2024. Adenosine and its receptors in the pathogenesis and treatment of inflammatory skin diseases. Int. J. Mol. Sci. 25, 5810. https://doi.org/10.3390/ijms25115810.

Cronstein, B.N., 2004. Adenosine receptors and wound healing. Sci. World J. 4, 1–8. https://doi.org/10.1100/tsw.2004.1.

Gomes Daré, R., Beatriz Chieco Costa, A., Silva Martins, T., Lopes, L.B., 2024. Simvastatin and adenosine-co-loaded nanostructured lipid carriers for wound healing: Development, characterization and cell-based investigation. Eur. J. Pharm. Biopharm. 205, 114533. https://doi.org/10.1016/j.ejpb.2024.114533.

Haskó, G., Cronstein, B., 2013. Regulation of inflammation by adenosine. Front. Immunol. 4. https://doi.org/10.3389/fimmu.2013.00085.

Haskó, G., Csóka, B., Németh, Z.H., Vizi, E.S., Pacher, P., 2009. A2B adenosine receptors in immunity and inflammation. Trends Immunol. 30, 263–270. https://doi.org/10.1016/j.it.2009.04.001.

Hassan, S., Ali, M.N., Mir, M., Ahmed, A., Arshad, M., 2021. Development and evaluation of drug delivery patch for topical wound healing application. SN Appl. Sci. 3, 825. https://doi.org/10.1007/s42452-021-04809-9.

Horvat, G., Pantić, M., Knez, Ž., Novak, Z., 2022. A brief evaluation of pore structure determination for bioaerogels. Gels 8. https://doi.org/10.3390/gels8070438.

Hoyer, H.W., Barrett, E.J., 1966. Differential thermal analysis of mixtures of DNA and nucleosides. Anal. Biochem. 17, 344–347. https://doi.org/10.1016/0003-2697(66)90213-2.

Hu, Y., Zhang, Q., You, R., Wang, L., Li, M., 2012. The relationship between secondary structure and biodegradation behavior of silk fibroin scaffolds. Adv. Mater. Sci. Eng. 2012, 1–5. https://doi.org/10.1155/2012/185905.

Jameson, J.F., Pacheco, M.O., Butler, J.E., Stoppel, W.L., 2021. Estimating kinetic rate parameters for enzymatic degradation of lyophilized silk fibroin sponges. Front. Bioeng. Biotechnol. 9. https://doi.org/10.3389/fbioe.2021.664306.

Jeong, Y., Patel, R., Patel, M., 2024. Biopolymer-based biomimetic aerogel for biomedical applications. Biomimetics 9, 397. https://doi.org/10.3390/biomimetics9070397.

Jin, Y., Zhang, S., 2024. Adenosine encapsulation and characterization through layer-by-layer assembly of hydroxypropyl-β-cyclodextrin and whey protein isolate as wall materials. Molecules 29, 2046. https://doi.org/10.3390/molecules29092046.

Kazemzadeh-Narbat, M., Reid, M., Brooks, M.-S.-L., Ghanem, A., 2015. Chitosan nanoparticles as adenosine carriers. J. Microencapsul. 32, 460–466. https://doi.org/10.3109/02652048.2015.1046517.

Kim, S.-K., Gao, Z.-G., Van Rompaey, P., Gross, A.S., Chen, A., Van Calenbergh, S., Jacobson, K.A., 2003. Modeling the adenosine receptors: comparison of the binding domains of A2A agonists and antagonists. J. Med. Chem. 46, 4847–4859. https://doi.org/10.1021/jm0300431.

Li, A.B., Kluge, J.A., Guziewicz, N.A., Omenetto, F.G., Kaplan, D.L., 2015. Silk-based stabilization of biomacromolecules. J. Control. Release 219, 416–430. https://doi.org/10.1016/j.jconrel.2015.09.037.

Lindholm, C., Searle, R., 2016. Wound management for the 21st century: combining effectiveness and efficiency. Int. Wound J. 13, 5–15. https://doi.org/10.1111/iwj.12623.

López-Iglesias, C., Barros, J., Ardao, I., Monteiro, F.J., Alvarez-Lorenzo, C., Gómez-Amoza, J.L., García-González, C.A., 2019. Vancomycin-loaded chitosan aerogel particles for chronic wound applications. Carbohydr. Polym. 204, 223–231. https://doi.org/10.1016/j.carbpol.2018.10.012.

Mallepally, R.R., Marin, M.A., McHugh, M.A., 2014. CO2-assisted synthesis of silk fibroin hydrogels and aerogels. Acta Biomater. 10, 4419–4424. https://doi.org/10.1016/j.actbio.2014.06.007.

Mallepally, R.R., Marin, M.A., Surampudi, V., Subia, B., Rao, R.R., Kundu, S.C., McHugh, M.A., 2015. Silk fibroin aerogels: potential scaffolds for tissue engineering applications. Biomed. Mater. 10, 035002. https://doi.org/10.1088/1748-6041/10/3/035002.

Marin, R.M., Franchini, K.G., Rocco, S.A., 2007. Analysis of adenosine by RP-HPLC method and its application to the study of adenosine kinase kinetics. J. Sep. Sci. 30, 2473–2479. https://doi.org/10.1002/jssc.200700194.

Marin, M.A., Mallepally, R.R., McHugh, M.A., 2014. Silk fibroin aerogels for drug delivery applications. J. Supercrit. Fluids 91, 84–89. https://doi.org/10.1016/j.supflu.2014.04.014.

Marks, R.M., Czerniecki, M., Penny, R., 1985. Human dermal microvascular endothelial cells: an improved method for tissue culture and a description of some singular properties in culture. In Vitro Cell. Dev. Biol. 21, 627–635. https://doi.org/10.1007/BF02623295.

Montesinos, M.C., Gadangi, P., Longaker, M., Sung, J., Levine, J., Nilsen, D., Reibman, J., Li, M., Jiang, C.-K., Hirschhorn, R., Recht, P.A., Ostad, E., Levin, R.I., Cronstein, B.N., 1997. Wound healing is accelerated by agonists of adenosine A2 (Gαs-linked) receptors. J. Exp. Med. 186, 1615–1620. https://doi.org/10.1084/jem.186.9.1615.

Montesinos, M.C., Desai, A., Chen, J.-F., Yee, H., Schwarzschild, M.A., Fink, J.S., Cronstein, B.N., 2002. Adenosine promotes wound healing and mediates angiogenesis in response to tissue injury via occupancy of A2A receptors. Am. J. Pathol. 160, 2009–2018. https://doi.org/10.1016/S0002-9440(10)61151-0.

Montesinos, M.C., Desai-Merchant, A., Cronstein, B.N., 2015. Promotion of wound healing by an agonist of adenosine A2A receptor is dependent on tissue plasminogen activator. Inflammation 38, 2036–2041. https://doi.org/10.1007/s10753-015-0184-3.

Naito M., Yokoyama T., Hosokawa K., Nogi, K. (Eds.), Structural Control of Nanoparticles. In: Nanoparticle Technology Handbook, Third Edition, Elsevier, 2018: pp. 49–107. DOI: 10.1016/B978-0-444-64110-6.00002-0.

Ng, W.Y., Migotto, A., Ferreira, T.S., Lopes, L.B., 2017. Monoolein-alginate beads as a platform to promote adenosine cutaneous localization and wound healing. Int. J. Biol. Macromol. 102, 1104–1111. https://doi.org/10.1016/j.ijbiomac.2017.04.094.

Oporto, K., Radojkovic, C., Mellisho, E.A., Zúñiga, F., Ormazábal, V., Guzmán-Gutiérrez, E., Nova-Lamperti, E., Rodríguez-Álvarez, L., Aranda, M., Escudero, C., Aguayo, C., 2023. Adenosine promoted angiogenesis mediated by the release of small extracellular vesicles from human endothelial progenitor cells. Microvasc. Res. 148, 104498. https://doi.org/10.1016/j.mvr.2023.104498.

Perez-Aso, M., Fernandez, P., Mediero, A., Chan, E.S., Cronstein, B.N., 2014. Adenosine 2A receptor promotes collagen production by human fibroblasts via pathways involving cyclic AMP and AKT but independent of Smad2/3. FASEB J. 28, 802–812. https://doi.org/10.1096/fj.13-241646.

Pritchard, E.M., Szybala, C., Boison, D., Kaplan, D.L., 2010. Silk fibroin encapsulated powder reservoirs for sustained release of adenosine. J. Control. Release 144, 159–167. https://doi.org/10.1016/j.jconrel.2010.01.035.

Ravichandran, V., Lee, M., Nguyen Cao, T.G., Shim, M.S., 2021. Polysorbate-based drug formulations for brain-targeted drug delivery and anticancer therapy. Appl. Sci. 11, 9336. https://doi.org/10.3390/app11199336.

Soorbaghi, F.P., Isanejad, M., Salatin, S., Ghorbani, M., Jafari, S., Derakhshankhah, H., 2019. Bioaerogels: synthesis approaches, cellular uptake, and the biomedical applications. Biomed. Pharmacother. 111, 964–975. https://doi.org/10.1016/j.biopha.2019.01.014.

Squadrito, F., Bitto, A., Irrera, N., Pizzino, G., Pallio, G., Minutoli, L., Altavilla, D., 2017. Pharmacological activity and clinical use of PDRN. Front. Pharmacol. 8. https://doi.org/10.3389/fphar.2017.00224.

Sultan, Md.T., Lee, O.J., Kim, S.H., Ju, H.W., Park, C.H. 2018. Silk Fibroin in Wound Healing Process, in: 2018: pp. 115–126. DOI: 10.1007/978-981-13-0947-2_7.

Szybala, C., Pritchard, E.M., Lusardi, T.A., Li, T., Wilz, A., Kaplan, D.L., Boison, D., 2009. Antiepileptic effects of silk-polymer based adenosine release in kindled rats. Exp. Neurol. 219, 126–135. https://doi.org/10.1016/j.expneurol.2009.05.018.

Tomeh, M.A., Hadianamrei, R., Zhao, X., 2019. Silk fibroin as a functional biomaterial for drug and gene delivery. Pharmaceutics 11, 494. https://doi.org/10.3390/pharmaceutics11100494.

Van Galen, P.J.M., Van Vlijmen, H.W.T., IJzerman, A.P., Soudijn, W., 1990. A model for the antagonist binding site on the adenosine A1 receptor, based on steric, electrostatic, and hydrophobic properties. J. Med. Chem. 33, 1708–1713. https://doi.org/10.1021/jm00168a027.

Wilson, C.N., Mustafa, S.J. (Eds.), 2009. Adenosine Receptors in Health and Disease, Springer Berlin Heidelberg, Berlin, Heidelberg. DOI: 10.1007/978-3-540-89615-9.

Wilz, A., Pritchard, E.M., Li, T., Lan, J.-Q., Kaplan, D.L., Boison, D., 2008. Silk polymer-based adenosine release: therapeutic potential for epilepsy. Biomaterials 29, 3609–3616. https://doi.org/10.1016/j.biomaterials.2008.05.010.

Yousaf, S.S., Houacine, C., Khan, I., Ahmed, W., Jackson, M.J., 2020. Importance of biomaterials in biomedical engineering. In: Advances in Medical and Surgical Engineering, Elsevier, pp. 151–177.